International Symposium of Research Students on Materials Science and Engineering
December 20-22, 2004, Chennai, India
Department of Metallurgical and Materials Engineering, Indian Institute of Technology Madras

PARAMETRIC STUDY OF CO_2/H_2S CORROSION OF CARBON STEEL USED FOR PIPELINE APPLICATION.

G. S. DAS & A. S. KHANNA
Corrosion Science & Engineering
Indian Institute of Technology Bombay
Powai, Mumbai- 400076

ABSTRACT

Four steels such as API X-52, API X-56, API X-60 and L-80 are generally used for pipeline application for carrying the crude oils and gas from offshore to different platforms. These steels are susceptible to internal corrosion in CO_2/H_2S environment. The comparison of corrosion resistance needs further investigation in the severe corrosive environment under dynamic condition. Few experiments have been carried out for corrosion studies in 3.5 % NaCl with liquid flow rate of 2.5 m/s. The corrosion rates were measured in the laboratory scale with simulating actual field condition in a closed autoclave loop system. The severity of their corrosion depends on various parameters such as pH, temperature, CO_2 partial pressure, H_2S concentration, dissolved oxygen and concentration of chloride. The temperature and partial pressure of CO_2 were varied from 30-120^oC and 50-300 psi respectively. The results indicate that as temperature and partial pressure of CO_2 increases, corrosion rate increases due to continuous dissolution of iron ion and formation of weak carbonic acid. The weak carbonic acid dissociates into carbonate and hydrogen ion, which increases the cathodic reaction on the metal surface. The presence of small amount of H_2S (0.4 ppm) increases the corrosion rate significantly. The corrosion rate of API X-60 grade steel shows better corrosion resistance compared to other steels. The corrosion products formed on the metal surface were analyzed by SEM, EDAX and X- ray diffraction techniques.

Key words: Autoclave, HTHP, CO_2 Partial pressure, Precipitation of $FeCO_3$

1. INTRODUCTION

Carbon steels are generally used for the petroleum industry for transportation of crude oils and gasses from offshore to different refining platforms and from their to different destination of the applications. The carbon steel is susceptible to internal corrosion due to CO_2/H_2S environment[1, 2]. The comparison of their corrosivity in the severe corrosive environment needs further investigation under the dynamic flow condition. The severity of corrosion depends on various working parameters such as partial pressure of CO_2, temperature, chloride concentration, H_2S level, surface films and oxide contents[4, 5]. There are very limited literatures available in the dynamic flow condition under H_2S environment[6]. The present study focused on some of the parameters, which affect the corrosion rates severely with multiphase flow condition. The surface films mainly consists of $FeCO_3$ and their influence on the corrosion rates were observed in CO_2 aqueous solutions [2, 3]. The formation of iron carbonate is temperature dependent and at higher temperature it forms the protective layers over the metal surface[7, 8]. The effect of H_2S on CO_2 saturated solution has been investigated by adding little amount of H_2S (0.4 ppm) in the same

working environment. The H_2S level from the surface has been easily skipped off due to the flow effect of liquid and the corrosion rate increases severely[7].

2. EXPERIMENTAL METHODS

The materials used for the experiments were supplied by Oil and Natural Gas Company limited (ONGC), Panvel, Mumbai and Essar Steel Limited Gujarat, India. The chemical composition of alloys, as obtained by inductively coupled plasma and atomic emission spectroscopy (ICP-AES) technique, are shown in Table 1.

The as received materials were cut into the rectangular specimens of dimension 12x10x2.5 mm with a hole of 1.5 mm diameter drilled near the top edge of each sample to facilitate suspension inside of an autoclave. The samples were polished to 600 grit emery papers, washed in distilled water and subsequently cleaned in acetone.

Experiments were carried out at four different temperatures (30, 60, 90 and 120^oC) at a constant partial pressure of CO_2 (50-300 psi) in 3.5% NaCl solution in a closed dynamic loop machine with a liquid flow velocity of 2.5 m/s. Initial weight of the samples (API X-52, API X-56, API X-60 & L-80) were measured and then suspended in specimen holder inside of autoclave. The vessel was deaerated by purging argon gas for 1-2 hours to maintain the oxygen impurity below 40 ppm. The oxygen level was measured by using the oxygen meter. The vessel temperature was increased to the testing condition by using silicon control rectifier (SCR), which supplies the heat to the vessel and then charged the partial pressure of CO_2 from the cylinder to maintain vessel pressure. The actual temperature of the vessel, solution and pressure inside the vessel were observed by digital display unit of the control panel. The loss of pressure during the operation was avoided by using the proper teflon tape. Each experiment was conducted using the same procedures for a total period of 24 hours with four fresh samples and corrosion rates were measured in mils per year (mpy). The corrosion products formed on the metal surface were analyzed by using X-ray diffraction (XRD) and scanning electron microscope (SEM) techniques.

3. RESULTS AND DISCUSSION

Corrosion rates of samples as a function of temperature obtained by the weight loss method are shown in Fig.1 to 2. The corrosion rates starts instantaneously still at low temperature due to continuous dissolution of Fe^{2+} ion in the solution. As the temperature increases corrosion rate increases due to the formation of porous iron carbonate films, results in the initiation of cracks and spallation of the oxide layers formed on the metal surface. The chloride ion easily ingress through the surface and significantly increases the corrosion at the temperature range of 60-90^oC. Further increase in temperature the corrosion rate decreases significantly due to the formation of denser, adherent and homogeneous layer of iron carbonate, which is, protects the metal to further corrosion. As the partial pressure of CO_2 in the solution increases the formation of weak carbonic acid (H_2CO_3) favors, which increases the corrosion rate. But at higher temperature the bicarbonate ions (HCO^{3-}) formed on the surface gives more carbonate ions (CO_3^{2-}) results in formation of more insoluble iron carbonate which increases the solution pH and corrosion rate decreases significantly as shown in Fig. 1-2 at 120^oC. In many literatures, it has been reported that $FeCO_3$ precipitation is temperature dependent and for its precipitation super saturation with the Fe^{2+} ion is required which is 5-10 times higher than the thermodynamically calculated values of solubility [7, 8, 9, 10].

The surface morphology of API X-52, API X-56, API X-60 and L-80 shows the rose bud, cactus, random carbonate globules and crack structures, which are not protective in nature at 90^oC as

shown in Fig. 3. However at 120°C the oxide films shows a very homogeneous network of iron carbonate distributed uniformly over the surface except some voids of the oxides in the case of API X-52 and L-80 grade steel and thus the metal remains protected from the further corrosion as shown in Fig. 4. Similarly in H_2S environments the structures of API X-52, API X-56, API X-60 and L-80 shows the elongated inclusions of MnS through which the cracks initiated which increases the corrosion rate due to localized attack at 90°C as shown in Fig. 5. However, the structures consist of rosebud and cactus structures surrounded by the homogeneous globules of $FeCO_3$, which strongly protects the surface at 120°C as shown in Fig. 6. The phases present in the oxide layers are mainly consist of iron carbonate ($FeCO_3$), magnetite (Fe_3O_4), hematite (Fe_2O_3) and iron sulphide (FeS), analyzed by XRD techniques and confirmed by the JCPDS files.

4. CONCLUSION

The solubility of iron carbonate is the function of bicarbonate anion concentration and the precipitation reaction, which depends on the system temperature. As the temperature increases the solubility of iron carbonate increases in the solution resulting in the precipitation of $FeCO_3$ on the surface and forms the protective layer as a local anode. The further precipitation of $FeCO_3$ can thus occur not only on the steel surface, but also directly on the local anode formed due to the ambient concentration in Fe^{2+} and the additional bicarbonate anions produced on that local anode by the cathodic reduction of CO_2. Hence a first consequence of the galvanic coupling between the steel and the local anode are therefore, the possibility of $FeCO_3$ precipitation at a certain distance from the steel surface, whereas in the absence of coupling it can only form on the steel surface, where the local Fe^{2+} and HCO_3^- concentrations are maximum and the homogeneous adherent and protective layers dominates on the metal surface and the corrosion rate decreases.

ACKNOWLEDGEMENTS

Authors thank to Institute of Engineering & Ocean Technology of Oil and Natural Gas Company limited (ONGC), Panvel, Mumbai and Essar Steel Limited Hazira, Gujarat, India for providing the materials for the current research work.

REFERENCES

1. E.W.J. van Hunnik, B.F.M. Pots, E.L.J.A. Hendriksen, "The Formation of Protective $FeCO_3$ Corrosion Product Layers in CO_2 Corrosion," CORROSION/96, paper no. 6 (Houston, TX: NACE, 1996).
2. Dugstad, "Mechanism of Protective Film Formation During CO_2 Corrosion of Carbon Steel," CORROSION/98, paper no. 31 (Houston, TX: NACE International, 998).
3. R. Nyborg, "Initiation and Growth of Mesa Corrosion Attack During CO_2 Corrosion of Carbon Steel," CORROSION/98, paper no. 48 (Houston, TX: NACE, 1998).
4. J.-L. Crolet, N. Thevenot, S. Nes¢ic, "Role of Conductive Corrosion Products on the Protectiveness of Corrosion Layers," CORROSION/ 96, paper no. 4 (Houston, TX: NACE, 1996).
5. K. Videm, A. Dugstad, Corrosion of Carbon Steel in an Aqueous Carbon Dioxide Environment. Part 2. Film formation, Mats. Perf. 28 (1989) 46–50.
6. C. DeWaard, U. Lotz, Prediction of CO_2 Corrosion of Carbon Steel, in : Prediction of CO_2 Corrosion in the Oil and Gas Industry, Institute of Materials Publisher, UK, 1994, pp. 30–49.
7. C. De Waard, U. Lotz, D.E. Milliams, Predictive Model for CO_2 Corrosion Engineering in Wet Natural Gas Pipelines, Corrosion 47 (1991) 976–985.
8. C.A. Palacios, J. R. Shadley, Characteristics of Corrosion Scales on Steel in a CO_2

Saturated NaCl brine, Corrosion 47 (1991) 122–127.
9. C. De Waard, D. E. Milliams, Carbonic Acid Corrosion of Steel, Corrosion 31 (1975) 177–181.
10. G.S. Das, A.S. Khanna, Corrosion Behavior of Pipeline Steel in CO_2 Environment CRSMS 03 /Transaction IIM June 04.
11. G.S. Das, A.S. Khanna, Corrosion Mechanism of Pipeline Steel in CO_2/H_2S Environment, NMD 2003
12. G.S. Das, A.S. Khanna, Role of H_2S on Corrosion behavior of micro alloyed pipeline Steel in CO_2 Environment, NML 2004
13. G.S. Das, A.S. Khanna, Effect of Hydrogen on Corrosion Behavior of Pipeline Steel in CO_2/H_2S Environment, NMD 2004
14. G.S. Das, A.S. Khanna, Life Prediction of Pipeline Steel in CO_2/H_2S Environment, NMD 2004
15. Role of Corrosion Products on the Protectiveness of Corrosion Layers for Micro Alloyed Pipeline Steel, Eurocorr 2004, (France, 12-15 September)

Table 1: Chemical composition of the alloys used (in wt%)

Grade	C	Mn	Si	S	P	Cr	Ni	Mo	Al	Cu
API X-52	0.09	1.31	0.25	0.006	0.012	0.009	0.07	0.003	0.03	0.08
API X-56	0.12	1.27	0.26	0.004	0.017	0.07	0.14	0.19	0.02	0.14
L-80	0.39	1.73	0.25	0.007	0.024	0.001	0.07	0.15	0.03	0.06
API X-60	0.07	1.48	0.27	0.004	0.013	0.09	0.02	0.008	0.04	0.20

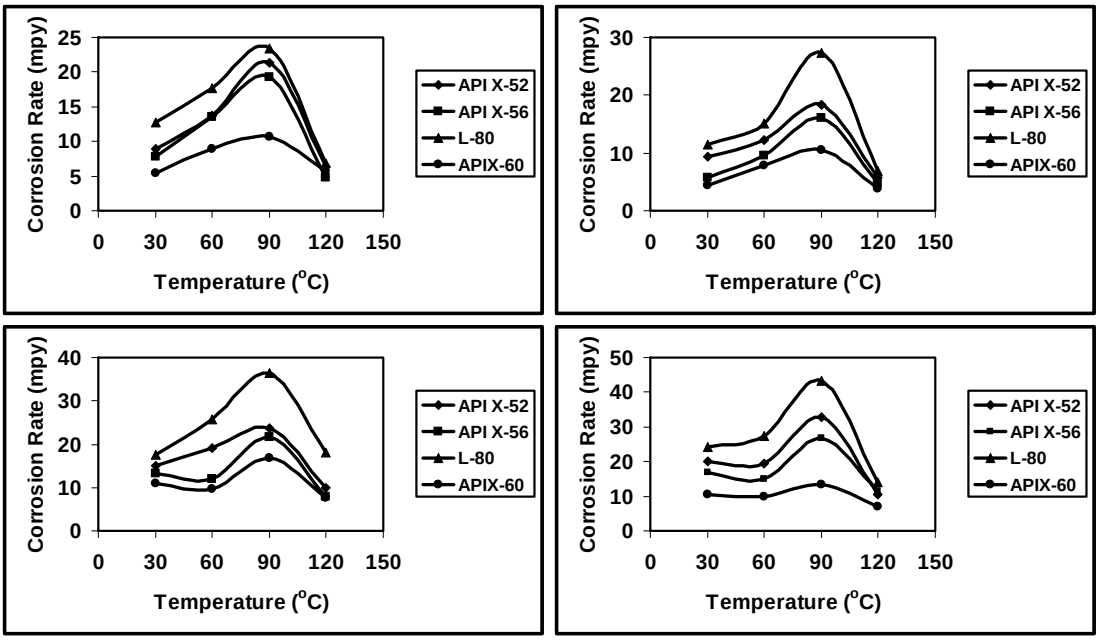

Fig. 1: Corrosion rate of samples exposed for 24 hrs. in 3.5 % NaCl, at a constant partial pressure of CO_2 (a) 50 psi (b) 100 psi (c) 200 psi (d) 300 psi and flow rate of 2.5m/s

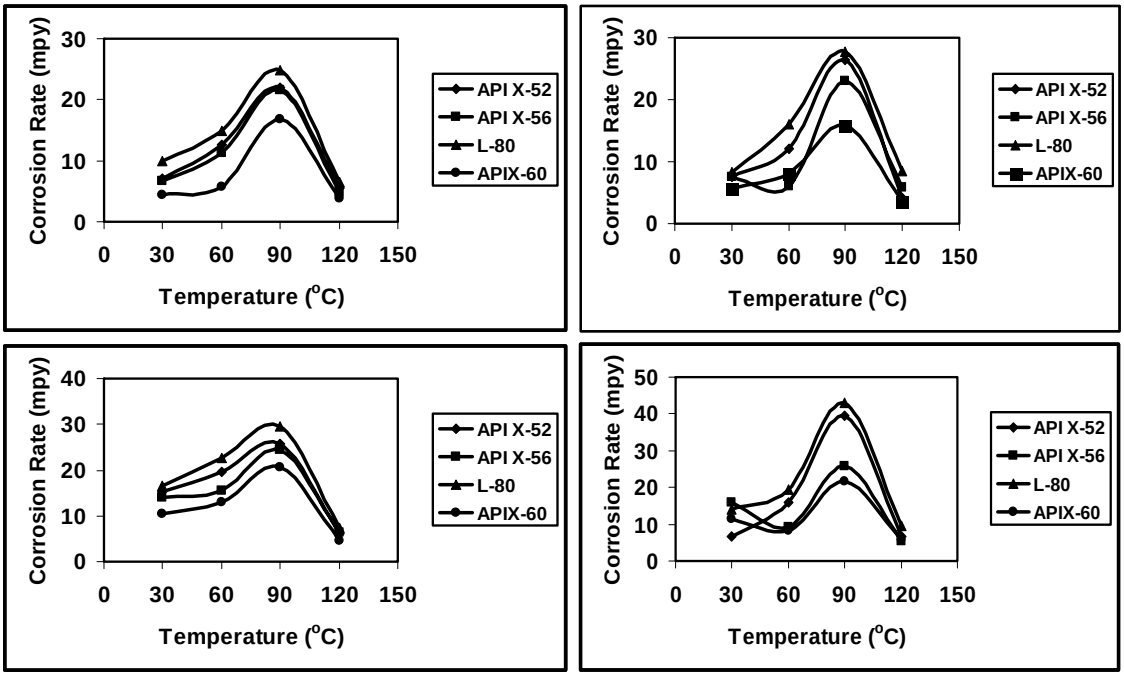

Fig. 2: Corrosion rate of samples exposed for 24 hrs. in 3.5 % NaCl, at a constant partial pressure of CO_2/H_2S (a) 50 psi (b) 100 psi (c) 200 psi (d) 300 psi and flow rate of 2.5m/s

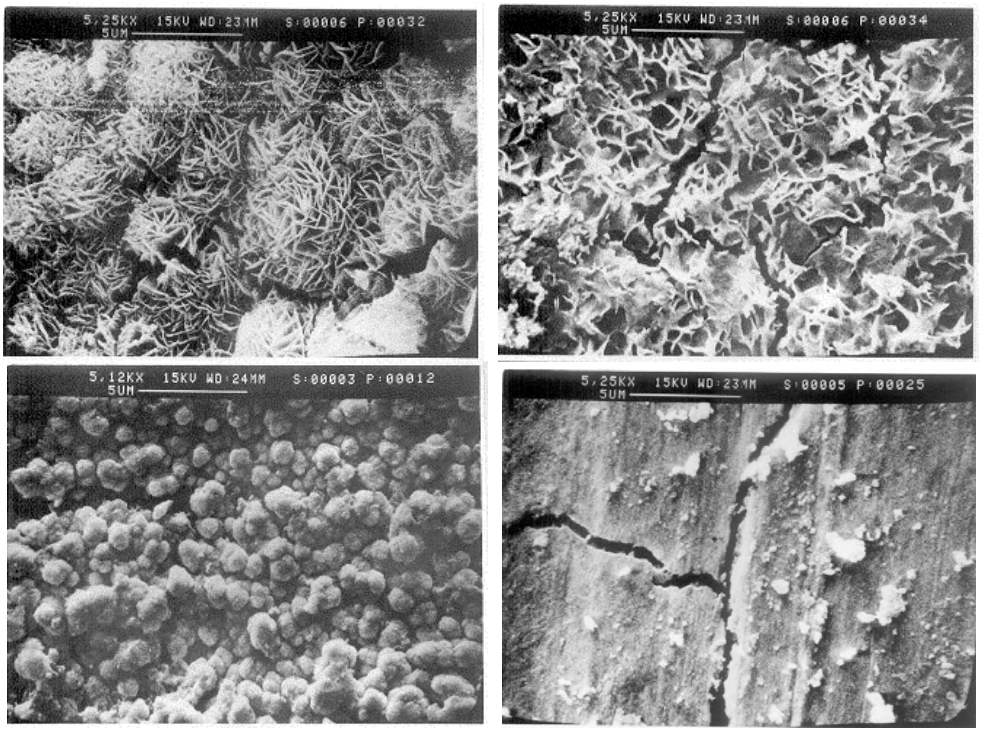

Fig. 3: SEM morphology of samples of (a) API X-52 (b) API X-56 (c) API X-60 and (d) L-80 at 90^{o}C after 24 hrs. exposed in 3.5 % NaCl with a velocity of 2.5 m/s

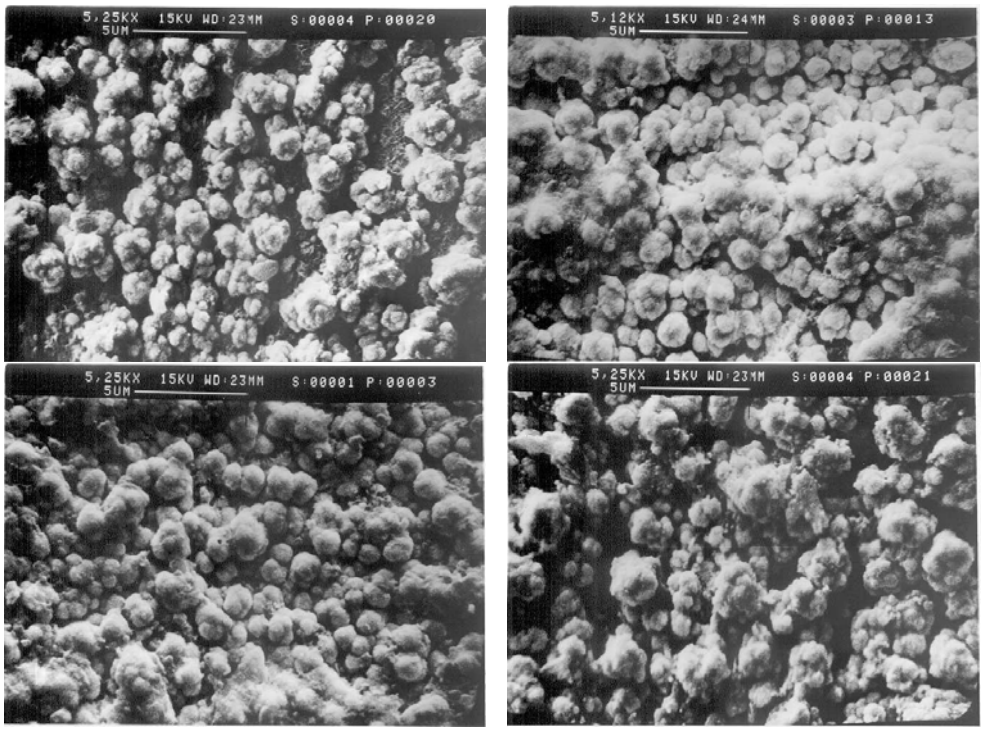

Fig. 4: SEM morphology of samples of (a) API X-52 (b) API X-56 (c) API X-60 and (d) L-80 at 120^{o}C after 24 hrs. exposed in 3.5 % NaCl with a velocity of 2.5 m/s

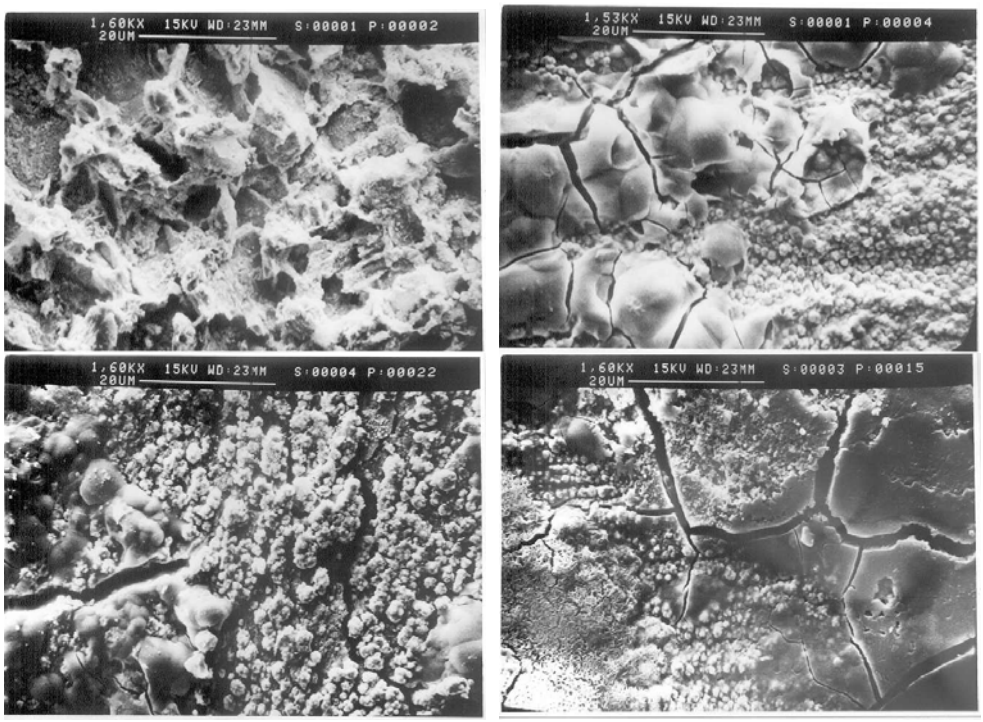

Fig. 5: SEM morphology of samples of (a) API X-52 (b) API X-56 (c) API X-60 and (d) L-80 at 90^{o}C after 24 hrs. exposed in 3.5 % NaCl with a velocity of 2.25 m/s

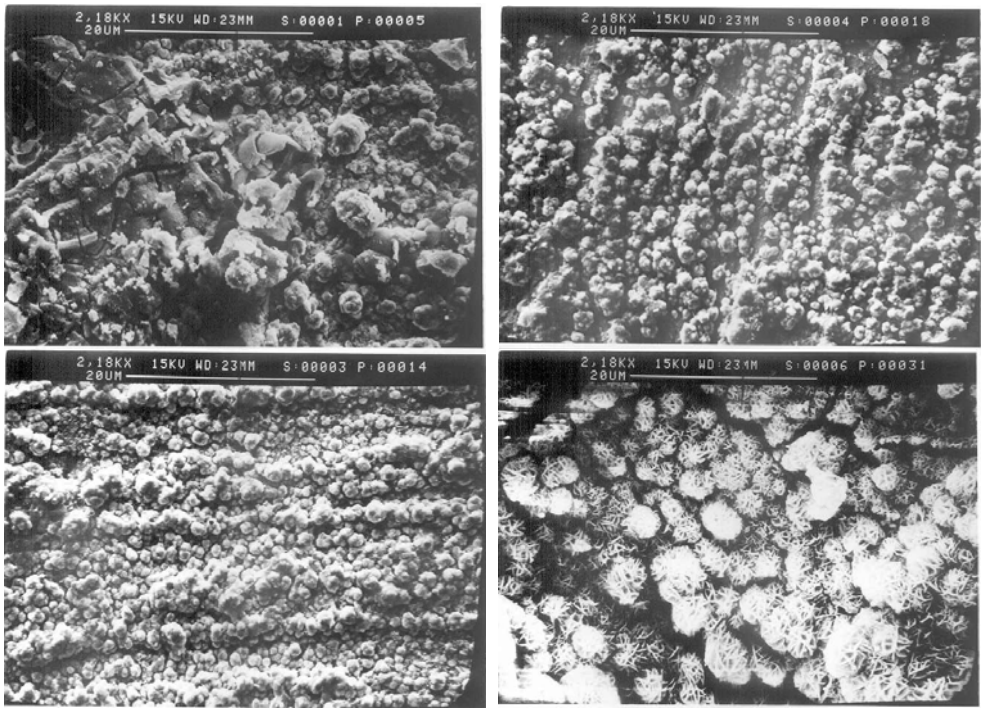

Fig. 6: SEM morphology of samples of (a) API X-52 (b) API X-56 (c) API X-60 and (d) L-80 at 120^{o}C after 24 hrs. exposed in 3.5 % NaCl with a velocity of 2.25 m/s

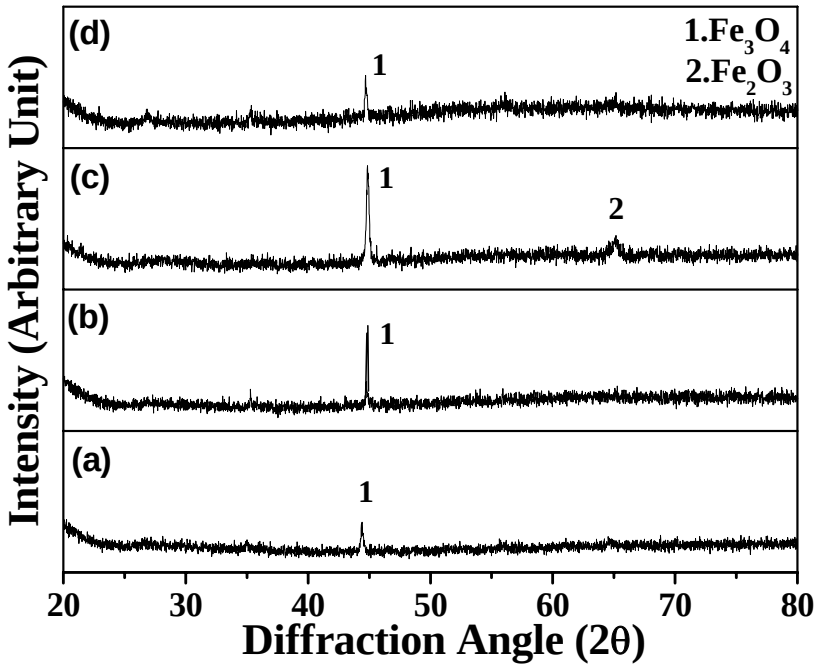

Fig. 7: XRD Patterns of the samples of (a) API X-52 (b) API X-56 (c) API X-60 and (d) L-80 in 90°C in CO_2 environment

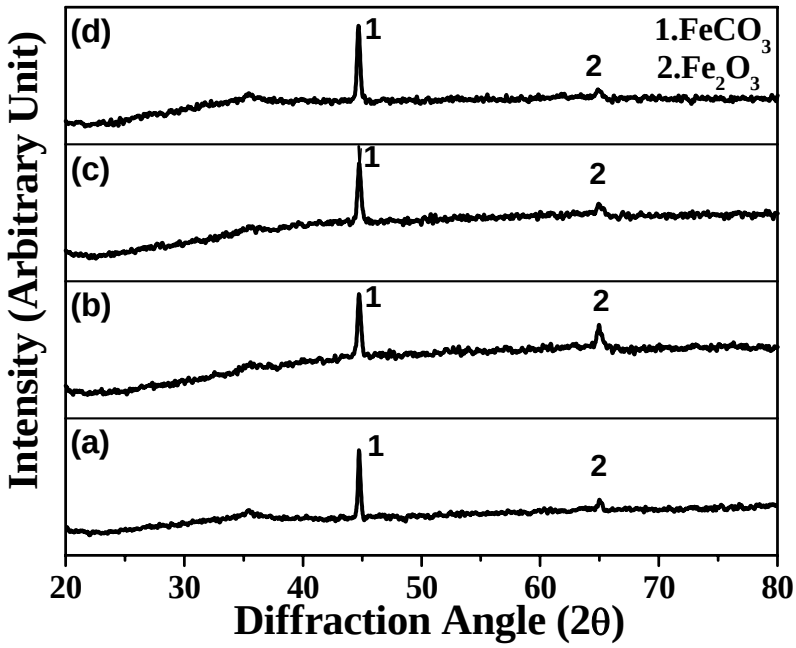

Fig. 8: XRD Patterns of the samples of (a) API X-52 (b) API X-56 (c) API X-60 and (d) L-80 in 120°C in CO_2 environment

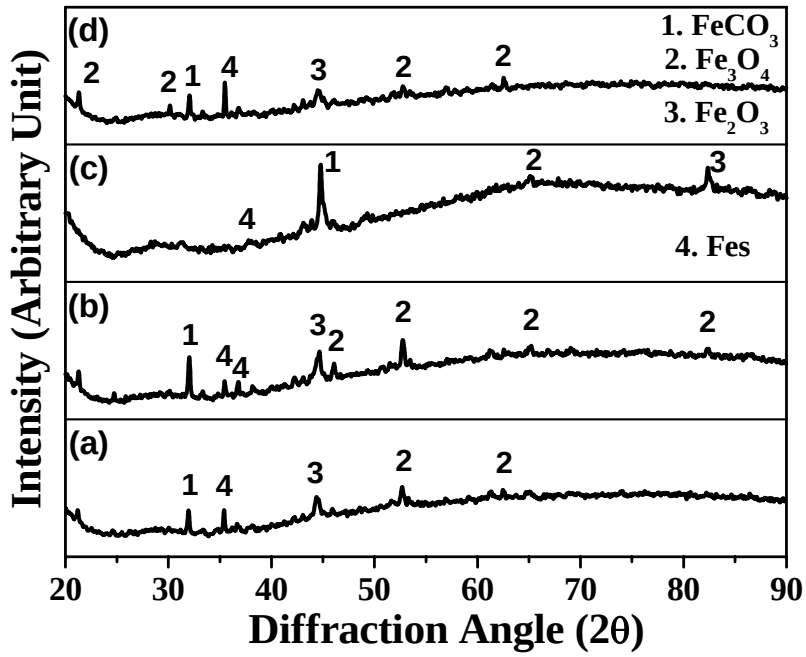

Fig.9: XRD Patterns of the samples of (a) API X-52 (b) API X-56 (c) API X-60 and (d) L-80 in 120°C in CO_2/H_2S environment

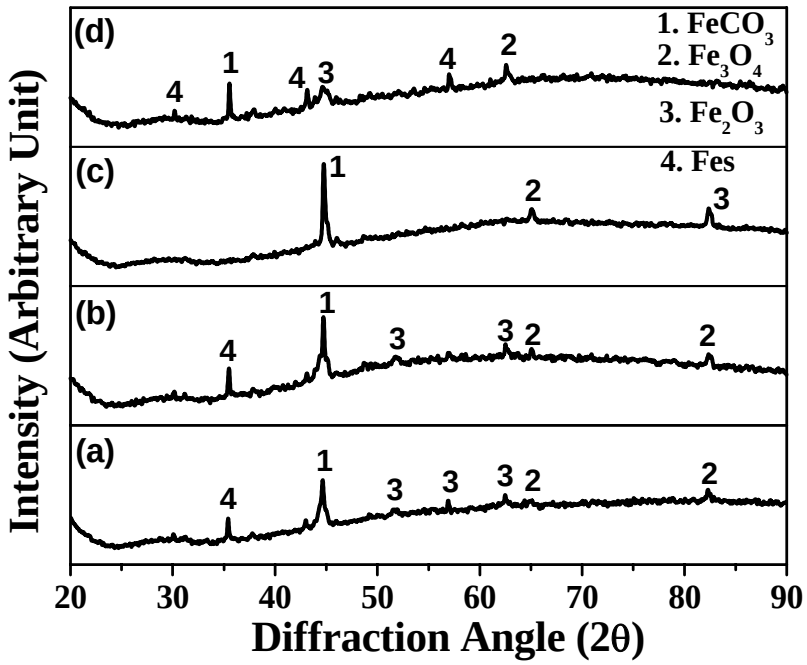

Fig. 10: XRD Patterns of the samples of (a) API X-52 (b) API X-56 (c) API X-60 and (d) L-80 in 120°C in CO_2/H_2S environment